Journal of Applied Polymer Science

Mixed-matrix membranes based on polyurethane containing nanohydroxyapatite and its potential applications

Gabriela Ciobanu,[1] Octavian Ciobanu[2]

[1]Faculty of Chemical Engineering and Environmental Protection, Gheorghe Asachi Technical University of Iasi, 63 Professor Doctor Docent Dimitrie Mangeron Road, Iasi 700050, Romania

[2]Faculty of Medical Bioengineering, Grigore T. Popa University of Medicine and Pharmacy, 16 Universitatii Street, Iasi 700115, Romania

Correspondence to: G. Ciobanu (E-mail: gciobanu03@yahoo.co.uk)

ABSTRACT: In this study, new asymmetric polyurethane (PU) mixed-matrix membranes with different nanohydroxyapatite loadings were prepared via a dry–wet phase inversion method by the dispersion of hydroxyapatite (HA) nanoparticles in the PU matrix. The HA nanopowder was obtained by a wet chemical precipitation method; it showed an average crystallite size of 58.3 nm, a specific surface area of 261 m^2/g, and a pore size of about 1.6 nm. The effects of the HA loading (10–50 wt %) on the PU membrane characteristics were studied. The scanning electron microscopy images revealed that the HA nanoparticles were well dispersed enough in the PU matrix. The average pore size in the top layer and porosity of the membranes slowly decreased, whereas the hydrophilicity and water permeability increased with increasing content of HA. The evaluation of the nanofiltration performance was performed by investigation of the NaCl rejection. The composite membranes had a higher salt-removal capacity than the unfilled PU membrane.
 J. Appl. Polym. Sci. **2015**, *132*, 41813.

KEYWORDS: composites; membranes; polyurethanes; porous materials; properties and characterization

Received 11 June 2014; accepted 25 November 2014
DOI: 10.1002/app.41813

INTRODUCTION

Membranes and membrane processes have become industrial products of significant technical and commercial importance. Membrane processes are effective for recovering valuable products, purifying aqueous process streams, simplifying wastewater treatment, and making further separation more attractive.[1] Membrane technology for water treatment has attracted widespread attention because of its low energy consumption. Among membrane technologies, the reverse osmosis and nanofiltration (NF) membranes have become one of the major means of water purification.

Synthetic membranes can be manufactured from a wide variety of materials, including polymers, metals, and ceramics. However, the vast majority of membranes in commercial use are based on polymeric materials. The permeability and selectivity characteristics of polymeric membranes are influenced not only by the molecular structure of the polymer but also by the physical structure or morphology of the membrane.[2] The structure of the membranes may be either symmetric or asymmetric. Fluid-separation processes require a membrane with high permeability and selectivity; these conditions are fulfilled by asymmetric membranes. The asymmetric membranes should have thin and dense skin layers supported by thick porous sublayers. These membranes are manufactured by phase-separation processes of homogeneous polymer solutions.[3]

The most common disadvantage associated with membrane application in the separation process is membrane fouling, which results in flux decline during operation. Membrane fouling could be reduced by the development of more hydrophilic membranes by membrane surface modification.[4] In recent years, a method used for this purpose is the incorporation of various kinds of nanoparticles into the polymeric membranes.[5] The resulting composite or hybrid membranes are referred to as *mixed-matrix membranes* (MMMs).[6] These membranes are a new class of materials that offer the potential of significantly advancing current technology because they are a promising alternative to conventional membranes.[7] The presence of finely dispersed inorganic nanoparticles (with their inherent superior separation characteristics) in the polymeric matrix has been proven to be very useful in the improvement of membrane properties and performances (antifouling, permeation, thermal stabilities, and mechanical properties) for a wide spectrum of processes, which range from gas separation and pervaporation to NF and ultrafiltration.[8–12]

Polyurethanes (PUs) are an important group of thermoplastic elastomers that are used as membrane materials and are known for their remarkable chemical and mechanical properties, such as resistance to extreme pH and temperature conditions, flexibility, tensile strength, and hardness.[13] These polymers are hydrophobic materials that consist of alternating hard and soft blocks that at microphase level, divide into hard and soft domains.[14] Practically, a right balance between hard and soft blocks provides a good separation process with no damage of the permeability. In recent years, some inorganic nanoparticles (silica, zeolites, etc.) have been introduced as fillers into the PU matrix to improve the permeation flux or selectivity of the PU membranes.[14–17]

One promising porous material for use as a filler for the fabrication of MMMs is hydroxyapatite (HA). The HA, $Ca_{10}(PO_4)_6(OH)_2$, is a calcium phosphate ceramic with important applications in the fields of medicine and chemistry. HA has been identified as a good adsorbent material for environmental processes because of its specific structure, which confers ionic exchange properties and adsorption affinity toward many pollutants.[18] This biomaterial has already been applied for the removal of heavy-metal ions and organic compounds (phenols, dyes, etc.) from water.[19,20]

In this study, new PU–nanohydroxyapatite porous MMMs with variable HA contents were prepared by a phase-separation process. The HA nanocrystals were dispersed within the PU matrix to improve their properties. The effects of the HA loading on the morphology, wettability, pure water flux (F), and solute rejection (R) of the resulting membranes were investigated.

EXPERIMENTAL

Materials

$Ca(NO_3)_2{\cdot}4H_2O$, $(NH_4)_2HPO_4$, NH_4OH, *N,N*-dimethylformamide (DMF), NaCl, and poly(ethylene glycol) (PEG) with molecular weights of 400, 600, 1000, 1500, and 4000 g/mol were purchased by Sigma-Aldrich (Germany). All chemicals and reagents were analytical grade. The PU polymer was supplied by the Institute of Macromolecular Chemistry "Petru Poni" of Iasi (Romania). The chemical structure of the PU is depicted in Figure 1. The hard-segment content in the PU was about 27.5 wt % and composed of 4,4′-diphenylmethane diisocyanate (MDI) and 1,4-butanediol (BD), and its soft segments consisted of poly(butylene adipate) (PBA). The hard segments contributed to the formation of the structural framework that provided mechanical support of the membrane. Instead, the soft segments formed microdomains composed of flexible chains that allowed the fluid transport and, therefore, provided good permeability

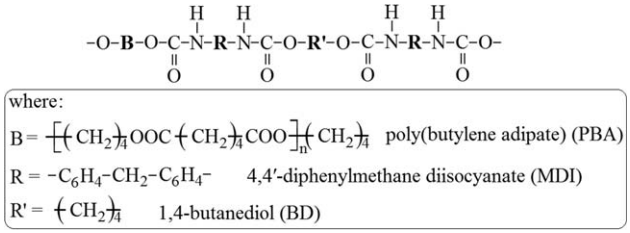

Figure 1. Chemical structure of the PU polymer.

to the membrane. The polar groups in the hard segments of PU were capable of bonding via hydrogen bonds with hydroxyl groups on the HA surface; thereby, this improved the ceramic polymer adhesion.

HA Nanopowder Synthesis

The wet chemical precipitation method was used to synthesize the HA nanopowder.[20] $Ca(NO_3)_2{\cdot}4H_2O$ and $(NH_4)_2HPO_4$ were used as calcium and phosphorous sources, respectively. An aqueous solution of 250 mL of $Ca(NO_3)_2{\cdot}4H_2O$ (0.01*M*) was added dropwise to an appropriate amount of an $(NH_4)_2HPO_4$ (0.006*M*) aqueous solution to achieve a predetermined Ca/P atomic ratio of 1.67. The solution was adjusted to pH 11 by the addition of small portions of NH_4OH (1*M*). The suspension was matured for 6 h at approximately 85°C under magnetic stirring. After that, the white powder was removed from the solution, washed with deionized water, and dried at 120°C for 24 h. The powder obtained was calcinated at 800°C to increase its crystallinity.

HA Nanopowder Characterization

The phase composition of the HA powder was characterized by X-ray diffraction (XRD) with an X'Pert PRO MRD diffractometer (PANalytical, The Netherlands) with monochromatic Cu Kα radiation ($\lambda = 0.15418$ nm). The average crystallite size was calculated from XRD data by the Scherrer equation with the peak at $2\theta = 25.9°$ for (002) reflection. The morphology and chemical composition of the sample were studied by scanning electron microscopy (SEM) coupled with energy-dispersive X-ray spectroscopy (EDX) with a Quanta 200 three-dimensional microscope (FEI, The Netherlands). Silver sputtering was used to make the coating surfaces conductive for the SEM investigations. The particle size distribution, ζ potential, and point of zero charge of the HA sample were measured with dynamic light scattering with a Zetasizer 3000 HS instrument (Malvern, United Kingdom). The wettability of the HA surface was estimated by the measurement of the contact angle with ultrapure water at ambient temperature with a DataPhysics OCA-H200 goniometer (DataPhysics, Germany). The HA powder was pressed into pellets (diameter = 8.5 mm, width = 3.5 mm) with an isostatic press. The specific surface area was evaluated by the fitting of the Brunauer–Emmett–Teller equation to the N_2 adsorption isotherms recorded by a Quantachrome Nova 2200e Win2 apparatus (Quantachrome, Germany). The pH measurements were realized with a Multi-Parameter Consort C831 (Consort, Belgium).

Membrane Preparation

The pure PU membrane (denoted PM-0) was prepared by the phase-inversion method with PU as the polymer, DMF as the solvent, and water as the nonsolvent, as described elsewhere.[16,17] The PU solution was made by the dissolution of a suitable quantity of polymer (30 wt %) in DMF at atmospheric pressure and 25°C for 6 h. Then, the polymer solution was cast on a glass plate at a designated wet thickness with a casting knife at ambient temperature and left subsequently for 5 min to form the skin layer. After that, the cast film was subsequently immersed into a coagulation bath containing distilled water at 10 ± 1°C for 10 min to complete the phase separation, where

Table I. Characteristics of the Unfilled and HA-Filled PU Membranes

Sample		PM-0	PHM-10	PHM-30	PHM-50
HA content (wt %)		0	10	30	50
Thickness (μm)[a]	Membrane	178	171	167	159
	Active layer	2.8	3.1	3.9	4.5
	Bottom layer	9.3	10.1	11.9	12.7
Pore diameter in the active layer	Maximum pore diameter (μm)[b]	1.4	1.2	0.9	0.7
	Effective pore diameter (nm)[c]	2.76	2.54	2.41	2.15
MWCO (g/mol)[c]		1730	1050	940	510
Pore diameter in the substructure (μm)[a]		30.5	32.7	35.8	37.7
Porosity (%)		74.3	72.6	68.4	67.1
Density (g/cm^3)		0.251	0.269	0.285	0.301
Contact angle (°)		91.63	82.41	73.52	69.34
WU (%)		27.9	78.4	109.8	114.2
F at 8 bar (L/m^2·h)		392.1	783.5	941.4	1110.7
Salt rejection at 8 bar (%)		81.4	88.1	93.8	97.1

[a] By the SEM method.
[b] By the bubble-point method.
[c] Determined by PEG permeation tests. The results in the table are average values.

exchange between the solvent (DMF) and the nonsolvent (distilled water) was induced. Finally, the membrane was heat-treated in a vacuum oven at 100°C for 12 h to remove the excess solvents (water and DMF).

The MMMs were obtained by the addition of a calculated amount of HA into the PU polymer solution and thorough mixing before casting. The weight percentages of HA loaded in each membrane were varied as stipulated in Table I. Special care was taken to ensure the homogeneous dispersion of the HA nanoparticles. To obtain optimal dispersions of the HA particles in the polymer solutions, stirring was required for at least 12 h. The mixture was sonicated for 30 min in a sonication cell to ensure homogeneous particle dispersion and to eliminate the trapped microbubbles. The casting and curing of the MMMs were identical with those of the PM-0. A series of flat-sheet membranes with loadings that varied between 10 and 50 wt % HA were made, and the most performant samples were denoted PHM-10, PHM-30, and PHM-50.

Membrane Characterization

The morphology of the membranes was studied by SEM with a QUANTA 200 three-dimensional microscope (FEI, The Netherlands). Fourier transform infrared (FTIR) spectroscopy was used to verify the HA incorporation in the PU matrix. IR spectra were collected in an FTIR Digilab Scimitar Series spectrophotometer (Digilab) with the attenuated total reflectance (ATR) technique. The scanning frequency range was 4000–600 cm^{-1}. The density measurements were performed with a Mettler AJ100 analytical balance fitted with a Mettler ME-33360 density determination kit on the basis of Archimede's Principle. The maximum pore sizes were estimated by the bubble-point method with a laboratory instrument. The porosity (ε) of the membranes was estimated by a gravimetric method by the weight of the liquid (isopropyl alcohol) contained in the membrane pores with the following equation:

$$\varepsilon = \frac{w_w - w_d}{\rho_w A l} \times 100 \quad (1)$$

where w_d is the weight of the dry membrane (g), w_w is the weight of the wet membrane after being dipped into isopropyl alcohol for 2 h (g), ρ_w is the isopropyl alcohol density (0.785 g/cm^3) at room temperature, A is the effective area of the membrane (m^2), and l is the membrane thickness (m).

The surface hydrophilic behavior of the membranes was tested with water contact angle measurements, whereas the bulk hydrophilicity was measured by a water uptake (WU) study. Water contact angle measurements (five measurements on different positions per sample, in triplicate, 2-mL drops of ultrapure water) were carried out with a DataPhysics OCA-H200 goniometer (DataPhysics, Germany), and each measurement was considered to have ±2° accuracy. The WU was investigated by the immersion of the membrane strips (2 × 5 cm^2) in distilled water for 24 h at room temperature (25°C) to ensure that the membranes were fully saturated. Then, membranes were dried in a vacuum oven at 70°C for 24 h and weighed. WU (%) of the membrane was calculated by means of the following relationship:

$$\mathrm{WU} = \frac{w_w - w_d}{w_d} \times 100 \quad (2)$$

Membrane Performance

The performance of the membranes was studied by checking their F values to determine the water-transport behavior of the membranes. Then, the membranes were subjected to a salt rejection study with a 2000-ppm NaCl feed solution with a pH of 9. The feed pH was adjusted by the addition of 0.1M NaOH. All of the permeation experiments were carried out in a

homemade dead-end flow cell with circular membranes with a 15-cm^2 effective area available for filtration. External pressure was applied with a nitrogen cylinder capable of producing up to 12 bar of pressure. Experiments were carried out at room temperature (25°C) at diverse pressures (1–8 bar) during a single run with the same membrane sample. Three coupons from each membrane were evaluated to determine F (L m^{-2}·h^{-1}) and R (%) as follows:

$$F = \frac{V}{At} \quad (3)$$

$$R = \left(1 - \frac{C_p}{C_f}\right) \times 100 \quad (4)$$

where V is volume of permeate collected (L), t is the sampling time (h), and C_p and C_f are the concentrations of the permeate and feed solutions, respectively. The feed and permeate concentrations were determined by conductivity measurements with a conductivity meter (Multi-Parameter Consort C831, Consort, Belgium).

The molecular weight cutoff (MWCO) of the obtained membranes was determined through permeation tests (at 8 bar) with PEGs with molecular weights of 400, 600, 1000, 1500, and 4000 g/mol as model solutes. The single-compound solutions (with only one PEG) were prepared by the dissolution of weighed amounts of PEG in salt-free distilled water at a concentration of 50 mg/L. The PEG concentrations in the feed and permeate were determined by gel permeation chromatography (Varian Co.). A plot of the rejection of each solute against the molecular weight allowed the MWCOs of the membranes to be estimated. The MWCO value of the membrane corresponds to the molecular weight of the PEG that is 90% rejected by the membrane.

The effective pore radius (r_p; nm) of the obtained membranes was evaluated according to the Donnan steric partitioning pore model developed by Bowen and Mukhtar.[21] This model is based on the extended Nernst–Plank equation and has often been used to characterize commercial NF membranes. The rejections of the neutral solute poly(ethylene glycol), with a molecular weight of 1000 g/mol [PEG1000; Stokes radius (r_s) = 0.784 nm], under different fluxes were measured by crossflow permeation tests. During the filtration experiments, the applied pressure was changed between 0 and 10 bar. A laboratory crossflow filtration apparatus was used in all of the experiments. The limiting observed PEG1000 rejection obtained from the rejection curve was taken as the limiting real rejection data ($R_{\lim}$), and r_p was calculated by the equation:[21]

$$R_{\lim} = 1 - \left(1 + 0.054\lambda - 0.988\lambda^2 + 0.441\lambda^3\right)(1-\lambda)^2 \quad (5)$$

where $\lambda = r_s/r_p$ is the ratio of Stokes solute radius to effective membrane pore radius.

The main characteristics of the prepared membranes are summarized in Table I.

RESULTS AND DISCUSSION

HA Characterization

The XRD method was applied to characterize the phase structure and crystallite size of the HA sample. The wide-angle XRD pattern in Figure 2 indicate that the calcined HA powder had characteristic peaks in the 2θ regions of 21–29, 32–34, 39–41, and 46–54°; this was in good agreement with the hexagonal HA phase (JCPDS Data Card 09–0432). The XRD peaks were well-defined; this indicated that the sample was crystallized well. The average crystallite size calculated by the Scherrer equation from the XRD line broadening was 58.3 nm.

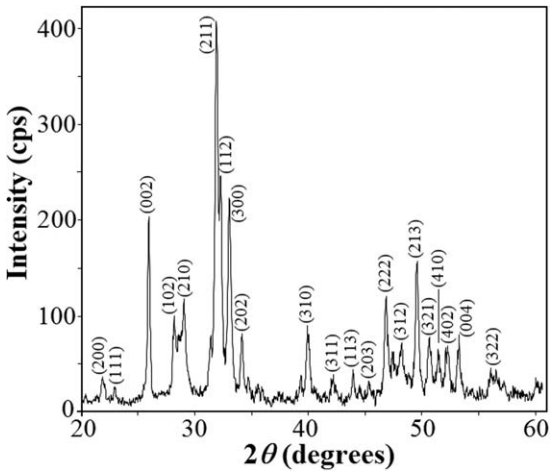

Figure 2. XRD pattern of the HA nanopowder.

The morphology of the HA sample is shown in the SEM micrograph [Figure 3(a)]. According to SEM image, the sample consisted of individual and some few aggregates of individual platelike crystallites. The agglomerates were perhaps formed by the coalescence of the crystals or by direct initiation at the

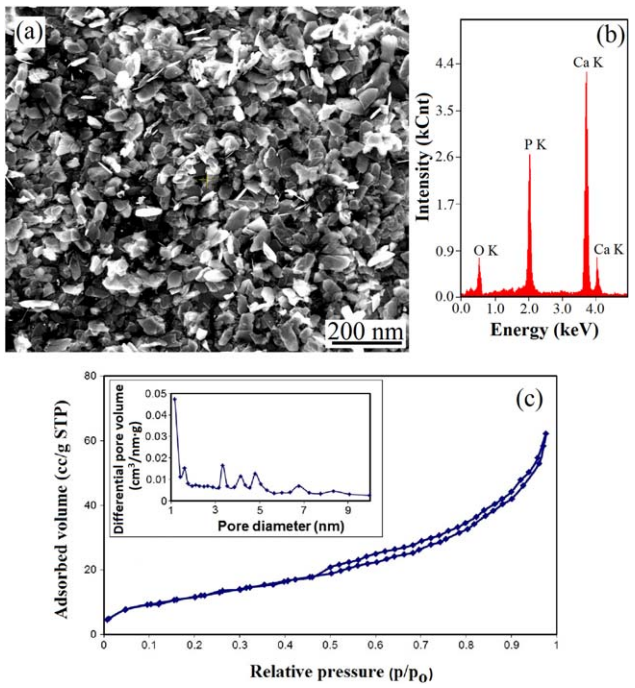

Figure 3. (a) SEM image, (b) EDX spectrum, and (c) adsorption isotherm (pore size distribution in the inset) of the HA nanopowder. kCnt, X-ray intensity in kiloCounts; p, equilibrium partial pressure of adsorbate; p_o, the saturated vapor pressure; dV(d), differential pore volume (cm^3/nm·g). [Color figure can be viewed in the online issue, which is available at wileyonlinelibrary.com.]

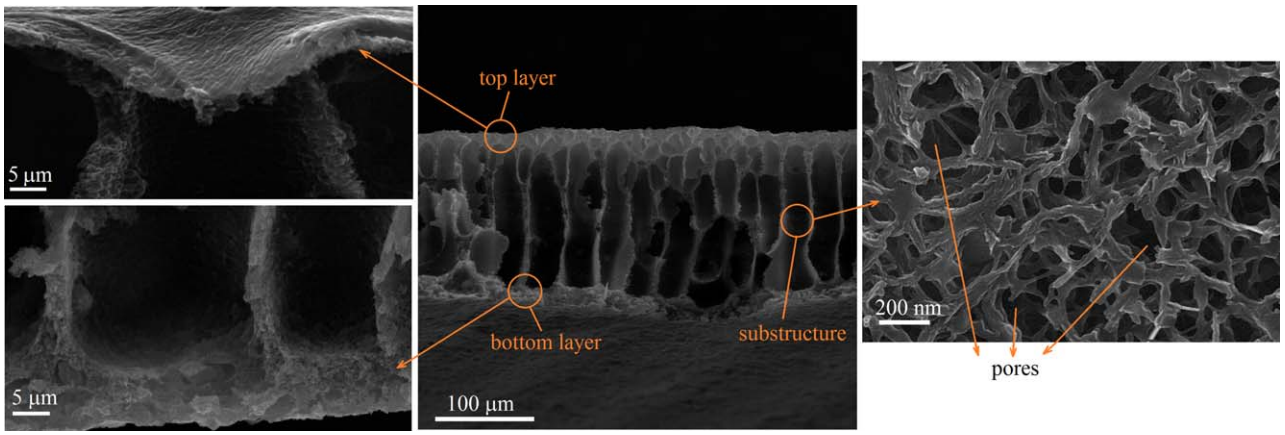

Figure 4. Cross-sectional SEM images (at different magnifications) of the PM-0 membrane. [Color figure can be viewed in the online issue, which is available at wileyonlinelibrary.com.]

contacting surfaces. The particle size measurements by dynamic light scattering indicated that the grain size distributions for the HA powder were situated within the nanometric range. The individual nanometric particles (average size ≈ 60 nm), with a percentage of about 78.5%, predominated over the particle agglomerations (average size ≈ 180 nm).

The EDX analysis confirmed the presence of Ca, P, and O in the HA crystallites [Figure 3(b)]. The Ca/P molar ratio was 1.663, mostly close to 1.67 and corresponding to the stoichiometric HA and to the $Ca_{10}(PO_4)_6(OH)_2$ formula.[22]

From the N_2 adsorption/desorption isotherm of the pure HA powder [Figure 3(c)], the Brunauer–Emmett–Teller surface area and pore volume were 261 m^2/g and 0.349 cm^3/g, respectively. The HA sample had micropores with an average pore diameter of about 1.6 nm.

The contact angle measurements with deionized water gave an average contact angle of 53.21°; this demonstrated that the HA surface was hydrophilic. The ζ potential of the HA sample was -19 ± 5 eV at pH 7.9, and the point of zero charge was found to be at pH 7.3. The literature indicates the existence of the positively ($\equiv CaOH_2^+$) charged sites in acidic pH media or negatively ($\equiv OPO_3H^-$) charged sites in basic pH media on the HA surface.[23,24] This indicated that the HA surfaces exhibited zwitterionic properties. Accordingly, the hydrophilic and negatively or positively charged HA surfaces (depending on the pH of the medium) played an important role in the enhanced separation properties.

Membrane Characterization

Membrane Structure. In this study, the phase-inversion process was used for the production of asymmetric MMMs. The SEM micrographs of the cross sections of the PM-0 and PHM-50 membranes at different magnifications are presented in Figures 4 and 5. The pictures for the other composite membranes were comparable to those of the PHM-50 membrane and, therefore, are not shown. As shown in the SEM images, each membrane had a skin (top) layer, a support porous layer (substructure), and a bottom layer with a fingerlike structure, which is the typical structure of an asymmetric NF membrane. The top layer acted as a selective barrier film for the solute in separation processes, whereas the porous substructure, which included macrovoids and micropores, offered excellent mechanical strength to the membrane and facilitating the liquid flow. As reported by Kesting,[25] generally large fingerlike macrovoids and cavity-like structures are formed when the coagulation process is fast, whereas the slow coagulation rate results in a porous spongelike structure. In our study, the coagulation took place fast (in ~15 min) when the polymer solution was brought into contact with cold water; this explained the fingerlike structure of the membranes.

All of the membranes showed uniform fingerlike pores linked by sponge walls in the substructure (Figures 4 and 5). The walls contained a large numbers of pores that allowed the fingerlike pores to communicate with each other. In the case of MMMs with these open-pore arrangements, an easy accessibility of foreign ions or molecules, which would interact with immobilized active sites of HA, is expected.

At shown in Figure 5 at high magnification, the cross section confirmed a good incorporation of the HA in the PU polymer matrix. The most HA particles were dispersed uniformly enough within the membrane substructure, except for very few clusters, which might have resulted from nanosized particles coalescing in the polymeric matrix. We assumed that the occurrence of these clusters was due to the fact that the surface of the HA contained OH functionalities (hydrophilic P—OH groups) and caused inherent hydrophilicity in these particles. Therefore, some HA nanoparticles tended to adhere to each other via hydrogen bonding, which formed some irregular agglomerations within the membranes.

The SEM images at high magnification (Figures 4 and 5) also indicated that all of the membranes had an active (skin) layer of about several micrometers in thickness. The formation of this layer is the key factor for the separation properties of the membranes and the molecular sieve property of membranes appeared to be determined by the pore size in the top layer. The skin layer possessed ultrafine pores with diameters much smaller than those of the supported layer (Table I). As shown in Table I, we found that an increase in the HA loading into the PU matrix resulted in a slow increase in the active layer thickness and a decrease in its

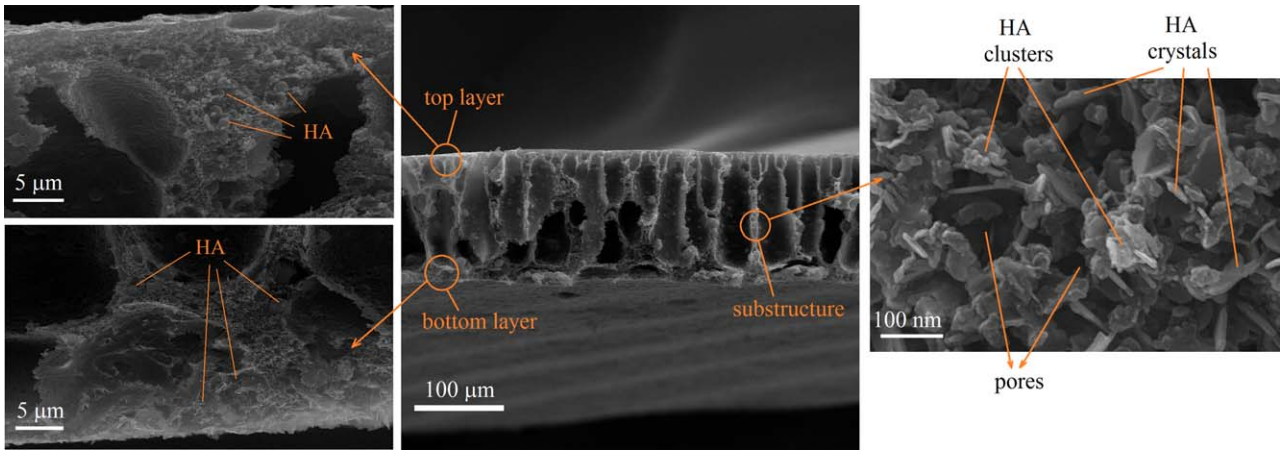

Figure 5. Cross-sectional SEM images (at different magnifications) of the PHM-50 membrane. [Color figure can be viewed in the online issue, which is available at wileyonlinelibrary.com.]

pore size. A possible explanation for the decrease in the pore size values was the increase in the viscosity of the casting solutions with the HA loading; this delayed the phase-inversion phenomenon. The increase in the viscosity typically delayed the exchange of solvent and nonsolvent and suppressed the formation of a large r_p. Also, this decrease in the pore size was explained by the existence of interfacial interactions between the PU matrix and the HA filler.

To study the effect of the HA content on the membrane structure the plane surface of the prepared membranes were also observed. The SEM image [Figure 6(a)] of the top surface of the PM-0 revealed a smooth structure with the presence of circular voids having a diameter of the order of several micrometers (2–7 μm). This was explained by the fact that in a certain zone of the film, the solvent was evaporated too fast. In the case of the MMMs, these voids decreased in size and

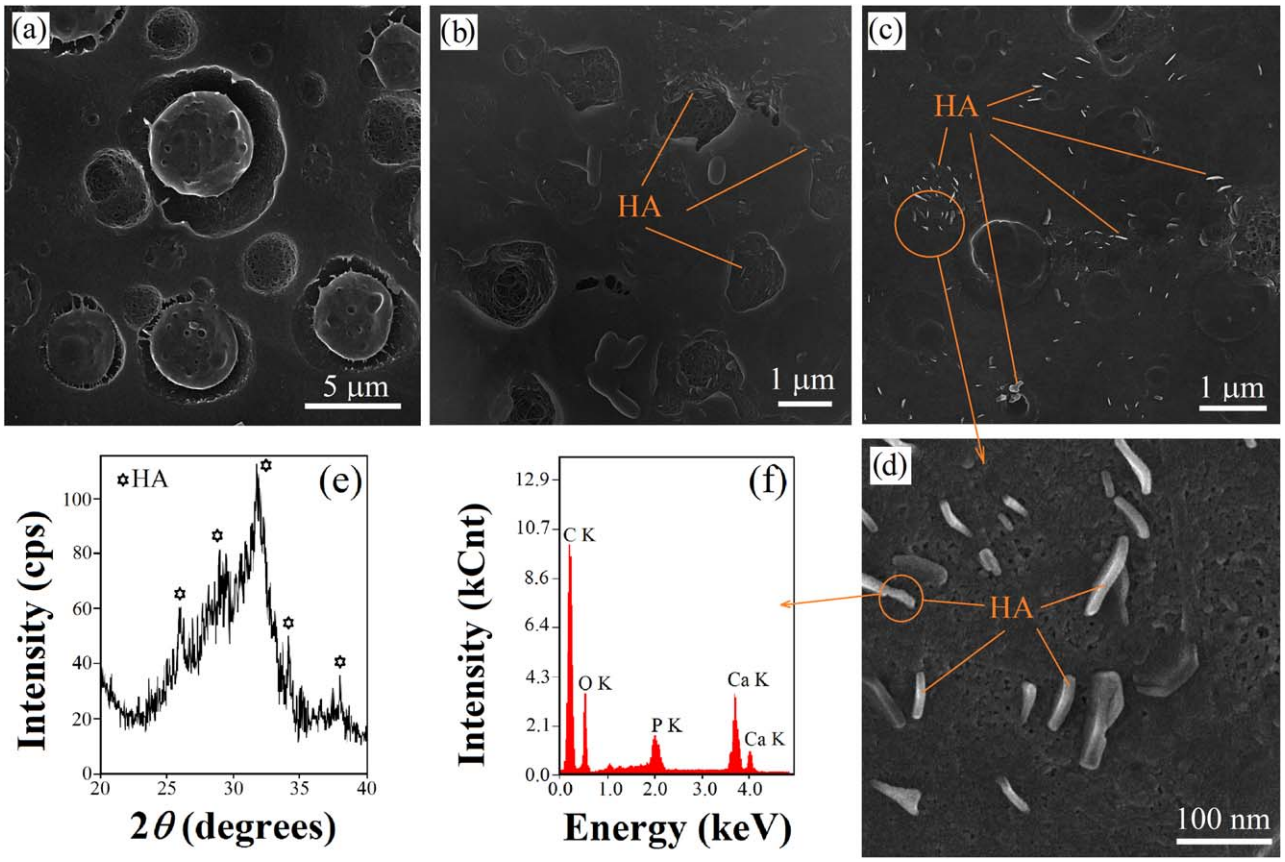

Figure 6. Surface views via SEM micrographs of (a) PM-0, (b) PHM-30, and (c,d) PHM-50 membranes and (e) XRD and (f) EDX spectra of the surface of the PHM-50 membrane. kCnt, X-ray intensity in kiloCounts. [Color figure can be viewed in the online issue, which is available at wileyonlinelibrary.com.]

number with increasing HA loading [Figure 6(b,c)]. We concluded that the visible surface improvement was due to the establishment of bindings between the PU matrix and the HA filler. Moreover, in Figure 6(d), the SEM image at higher magnification showed that the polymer adhered well to the HA particles and that no voids were present around these particles. The literature indicates that HA crystals are covered with weakly acidic surface P—OH groups that show favorable interactions with organic molecules through hydrogen bonds.[26] Therefore, in the MMMs, it was possible that hydrogen-bonding interactions occurred between the polar groups of PU and the surface P—OH groups of HA; this was supported by the results of the FTIR analysis. This would suggest that linkages between the PU polymer and HA were successful in promoting adhesion between the two components.

During the MMM preparation, the agglomeration of nanoparticles due to sedimentation or migration to the membrane surface is a factor of a great importance.[8] Some filler particles may migrate to the membrane surface and agglomerate. Mahajan *et al.*[27] assumed that the filler agglomeration at the surface was the result of convection cells that were formed during the casting of the film. In this study, on the membrane surface, some small HA crystals were observed, especially for the MMMs with high HA contents [Figure 6(b–d)].

In contrast to migration to the membrane surface, because of the difference in the physical and chemical properties between the filler and polymer, the sedimentation of filler crystals could occur during the MMM preparation as a result of the formation of inhomogeneous filler and polymer phases in the filled membrane.[8] This situation was especially serious when the filler loading in the MMM was higher. To prevent this phenomenon, the literature indicated the use of fillers with very small particles (<0.5 μm).[28] Therefore, in this study, we used ultrafine HA crystallites (<200 nm) with a consequent reduction in the sedimentation rate in the filled membrane. The SEM micrographs illustrated that generally, the HA nanoparticles were well dispersed enough in the PU matrix in all of the samples without visible sedimentation in the bottom layer (Figures 4 and 5). On the other hand, for higher HA contents, the bottom layer became thicker.

As shown in Figure 6, the XRD and EDX spectra of the surface of the PHM-50 membrane are also shown. The XRD pattern [Figure 6(e)] of the surfaces of the PU/HA membrane showed the broad peaks assigned to HA around 23 and 35° in the 2θ range; this indicated that the crystalline deposits observed as white spots under SEM [Figure 6(b–d)] were crystalline HA. The EDX spectrum [Figure 6(f)] also showed the presence of HA on the PU surface due to the existence of the characteristic peaks (Ca, P, O) related to HA crystals. Additionally, the high-intensity signal of the carbon (C) element was due to the PU matrix.

These findings indicated that the addition of the nanosized HA particles at a load of up to 50% did not affect the inner finger-like structure of the membranes. As shown in Table I, a slight reduction in the membrane thickness and porosity of the membrane was distinguished when the amount of HA added to the

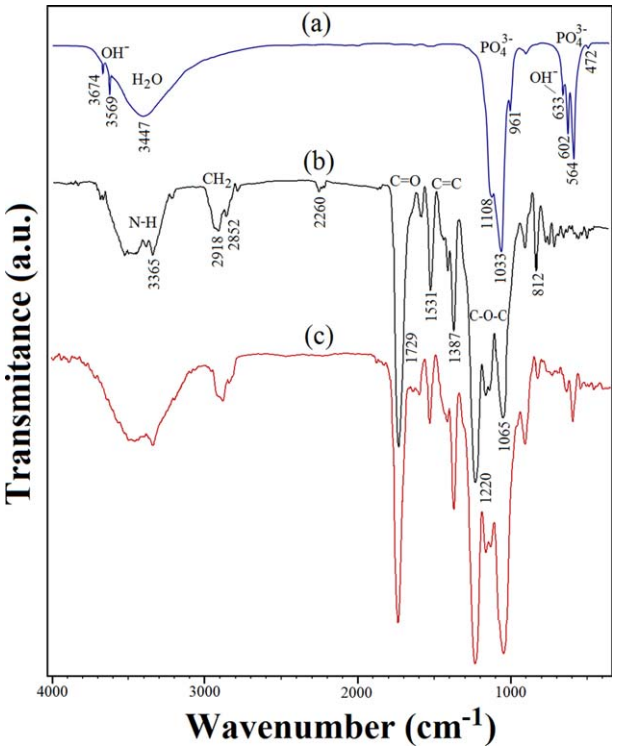

Figure 7. FTIR spectra of the (a) HA nanopowder and (b) PM-0 and (c) PHM-50 PU membrane samples. [Color figure can be viewed in the online issue, which is available at wileyonlinelibrary.com.]

PU matrix was increased. An increase in the HA loading into the films may have resulted in a slight increase in the MMM density, as shown in Table I. This increase was attributed to both the interfacial interactions between PU and HA and the homogeneous dispersion of HA particles in the PU matrix. Similar results were also reported in the literature.[29]

The brittleness of the final membranes was influenced by the amount of HA in the MMMs. When the amount of HA particles in the composites was less than 50%, the obtained membranes were intact and strong. We noted that these wet membranes with various compositions (<50% HA) displayed good flexibility and became easy to manipulate when immersed into water because of the hydrophilic properties of HA. On the other hand, when the amount of HA was higher than 50%, the membranes possessed a relatively coarse surface and became brittle. For this reason, these membranes could not be studied.

FTIR Spectra. The FTIR spectra of the pure HA powder and PU membrane were compared with those of the MMMs. The FTIR spectrum of the HA nanoparticles [Figure 7(a)] showed adsorption bands around 472, 564, 602, 961, 1033, and 1108 cm^{-1} and corresponded to the phosphate (PO_4^{3-}) polyhedrons in the HA structure.[26] The 3674-cm^{-1} band was assigned to the surface P—OH groups; the sharp peak at 3569 cm^{-1} to the stretching vibrations of the lattice OH^- ions and the medium sharp peak at 633 cm^{-1} to the O—H deformation mode. The broader band at 3447 cm^{-1} was attributed to the water molecules adsorbed on the surface of HA.

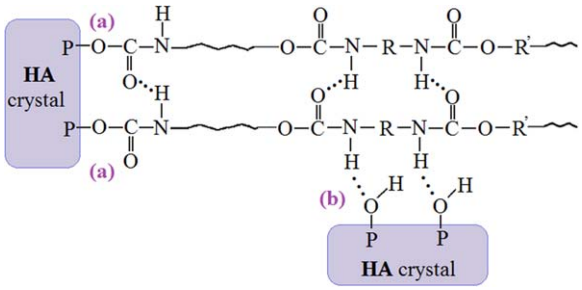

Figure 8. Possible (a) chemical and (b) physical linkages in the HA–PU MMMs. [Color figure can be viewed in the online issue, which is available at wileyonlinelibrary.com.]

The FTIR spectrum of PM-0, depicted in Figure 7(b), confirmed the PU structure.[30] The N—H stretching vibrations of urethane occurred at approximately 3365 cm^{-1}, and the stretching vibrations of free carbonyl (C═O) groups occurred at 1729 cm^{-1}. The carbonyl group involved in hydrogen bonding is known to absorb at about 1600–1670 cm^{-1}. The 2260-cm^{-1} band was assigned to the terminal isocyanate (—N—C═O) groups. The peaks of the urethane ether linkage (C—O—C) were found at 900–1230 cm^{-1}. Intensive absorption bands at 3000–2800 cm^{-1} corresponded to the symmetric and asymmetric bending oscillations of CH_2 groups. The peaks assigned to the C═C aromatic stretching appeared at 1380–1510 cm^{-1}. The other characteristic bands were noticed at 1174 cm^{-1} due to the coupled C—N and C—O stretching vibrations and at 812 cm^{-1} due to the C—O out-of-plane bending.

In case of the MMMs, the FTIR spectra were recorded to investigate the changes in the chemical environment between the PU polymer chains and HA crystals. Thus, the FTIR spectrum of the PHM-50 sample depicted in Figure 7(c) indicated the presence of the characteristic absorption peaks of HA and PU and some molecular interactions between PU and HA. Figure 8 showed possible crosslinking in the HA–PU MMMs. In the FTIR spectrum, we observed that the absorption peaks at 3569 and 2260 cm^{-1} (representing the bending vibrations of the hydroxyl groups of HA and terminal isocyanate groups of PU, respectively) were not to be found. This means that chemical linkages were formed between the OH groups on the surface of the HA nanocrystals and the N—C═O groups of PU [as also depicted in Figure 8(a)]. Moreover, the hydrogen bonds between the N—H groups of the PU polymer and P—OH groups of HA were made evident by the presence of a broad band at 3300–3500 cm^{-1}. This band was slightly wider in the composite membrane; this indicated that extra hydrogen bonds were established between the OH groups on the surface of the HA and the N—H groups of the PU chains [as depicted in Figure 8(b)], with a partial destruction of the hydrogen-bond associations within polymer chains. In conclusion, these interactions prevented the detachment of the PU chains from HA nanocrystals, as shown in the SEM images [Figure 6(d)].

Water Contact Angle and Water Absorption. Generally, the introduction of hydrophilic inorganic particles to a hydrophobic polymer membrane can improve the hydrophilicity of the membrane surface and pore walls.[31] Because the HA powder used in this study had a hydrophilic state with a contact angle of 53.21°, an additional measurement of contact angle was performed to investigate the effect of HA loading on the membrane hydrophilicity. As shown in Table I, the water contact angle decreased evidently from about 91.63 to 69.34° with increasing HA loading from 0 to 50 wt %; this indicated an increased surface wettability. The presence of HA in the PU matrix led to changes in the character of the PU membrane surfaces from hydrophobic to hydrophilic and thus increased the wetting properties of the MMMs because of the polar groups of the HA hosted on the PU surface.

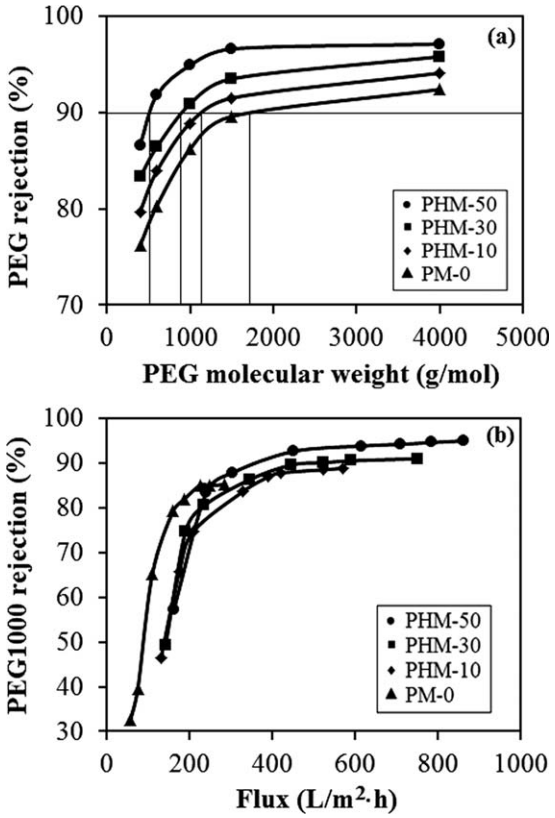

Figure 9. (a) PEG rejection of the PU membranes with PEGs of different molecular weights at 8 bar and (b) PEG1000 rejection versus the flux (50 mg/L PEG aqueous solution, 25°C).

As known, WU measurements are important for understanding the hydrophilic properties of membranes. The WU of the membrane depends especially on two factors: the number of hydrophilic sites present in the membrane matrix and the membrane morphology (i.e., the macrovoids present in the polymeric substructure). We noticed from the results in Table I that the WU increased as the HA loading increased in the PU matrix; this revealed an increase in the hydrophilic sites in the PU matrix. So, we concluded that the affinity of the membrane toward water increased with increasing HA content. Thus, it was quite clear that the HA surface contained hydrophilic sites; this facilitated the uptake of water into the membrane matrix. Being a zwitterionic material, the HA could bind water molecules more strongly than other hydrophilic materials via electrostatically induced hydration.[32] Also, from Table I, we observed that the HA loading resulted in a slow increase in macrovoids in the

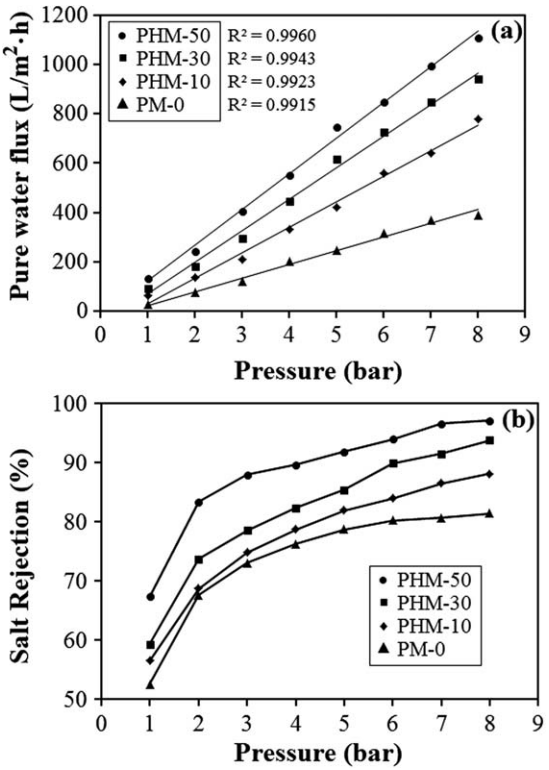

Figure 10. Effect of the pressure on (a) F and (b) NaCl rejection for the prepared membranes at 25°C and after 60 min of filtration (R^2 = correlation coefficient).

membrane substructure. This was why the MMMs could accommodate more water molecules and thus increase the overall uptake capacity.

MWCO and Effective r_p of the Membranes. The retentions at 8 bar for the five different PEG fractions are presented in Figure 9(a). As shown in this figure, the MWCOs of the PM-0, PHM-10, PHM-30, and PHM-50 membranes were about 1730, 1050, 940, and 510 g/mol, respectively (Table I).

The PEG1000 rejection as a function of flux for the PU membranes is presented in Figure 9(b). As shown in this figure, we found that the PEG1000 R_{lim} of the PM-0, PHM-10, PHM-30, and PHM-50 membranes were about 85.21, 88.86, 90.99, and 94.98%, respectively. The values of the calculated r_p values of the PU membranes were 1.38, 1.27, 1.20, and 1.07 nm, respectively (the effective pore diameters of the PU membranes are presented in Table I).

The results indicate the tendency of the decreasing membrane pore size of the formed composite membrane with increasing HA content in the PU matrix.

Membrane Performances. The separation performances of the prepared membranes were described in terms of the water flux and salt rejection, and the results are summarized in Table I and Figure 10.

F was measured at different pressures (1–8 bar) to ensure that the used membranes were stable. According to Figure 10(a), for all of the membranes, F increased linearly with increasing applied pressure. Consequently, these membranes were stable in the producing flux and were suitable for the further applications. Table I and Figure 10(a) show that the F values of the MMMs were greatly enhanced with increasing HA loading. This was due to the fact that the hydrophilicity of the composite membranes was improved by the addition of the porous HA; this could produce many hydrophilic pores with nanometer sizes of about 1.6 nm in the thin film layer and pore walls of the MMMs. The MMMs showed a significant improvement in water flux performance (and water permeance) compared to PM-0. This might have been due to the incorporation of the HA phase, which showed a hydrophilic nature, surface charge (negatively or positively charged surface, depending on the pH of the medium), molecular sieve effect, and larger resistance to swelling. Similar results have also been reported in the literature.[33–36]

The permeation experiments were conducted with a 2000-ppm NaCl solution at pH 9 and at diverse pressures (1–8 bar). In Figure 10(b), the increase in the NaCl rejection with increasing applied pressure is shown. All of the prepared membranes showed a high salt rejection, which was greater than 81% at 8 bar of pressure (Table I). However, the rejection capability of the prepared MMMs was higher than that of the unfilled PU membrane. This was due to the existence of the negatively ($\equiv OPO_3H^-$) charged sites on the HA surface in basic media, as mentioned before. Hydrophilic and negatively charged HA surfaces played an important role in the enhanced separation properties because these surfaces are highly attractive to water but highly repulsive to anions due to the columbic repulsion. At pH 9, where the membrane pore was more negatively charged, the Cl^- (the co-ion) experienced electrostatic repulsion from the membrane pores and was rejected by the composite membrane. Because the electroneutrality of the permeate solution had to be maintained, the Na^+ was also rejected. The high R of the MMMs indicated that the ion did not pass through the membrane. The membrane surface was negative in nature; hence, the Donnan exclusion principle played a significant role in governing the rejection of charged inorganic solutes.

The fouling behavior of the membranes was also studied. The flux of the membranes was investigated for a period of 12 h at a constant pressure (8 bar) with a feed solution of 2000-ppm NaCl at pH 9 during a single run. Figure 11 shows that the permeation flux declined as the filtration time increased; this was

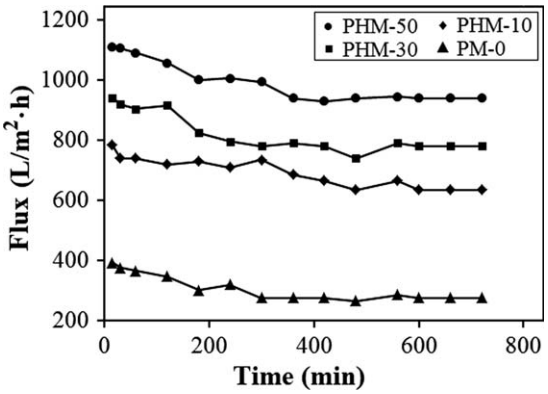

Figure 11. Permeate flux over time for the prepared membranes at 25°C and 8 bar with a 2000-ppm NaCl feed solution (pH 9).

followed by a period at a steady value. This could be explained by membrane fouling. The flux decline was no more than 19% for the composite membranes; the lowest value was 15.36% for the PHM-50 sample compared with 29.86% for the unmodified PU membrane (PM-0 sample). This showed that the composite membranes had a more favorable antifouling performance. As demonstrated previously, the incorporation of the HA particles into the PU matrix enhanced the hydrophilicity of the composite membranes and resulted in an enhanced fouling resistance.

Consequently, the presence of the HA particles in the PU membranes improved the membrane performance in terms of their flux and fouling resistance.

Finally, the results of this study indicate that the asymmetric PU/HA MMMs could potentially be used in separation applications. However, additional studies are needed to elucidate the transport mechanisms of the separation process in the PU/HA MMMs. Future research shall further explore the rejection of trace organic and inorganic contaminants. This could be useful in future process optimization and could be used as a tool to improve the development of specific membrane applications.

CONCLUSIONS

New MMMs based on nanohydroxyapatite and PU were prepared via a dry–wet phase inversion method. These composites were defined as a synergistic combination of the PU polymer with the HA inorganic nanofiller dispersed at the nanometer level. The HA nanoparticles were embedded in the PU matrix by blending in the casting solution. The improved properties of the MMMs resulted from favorable interfacial interactions between the HA nanoparticles and the PU polymer. All of the membranes showed uniform fingerlike pores linked by sponge walls in the substructure. The SEM–EDX, XRD, and FTIR studies of the composite membranes confirmed the presence of HA nanocrystals in the PU matrix, with the latter showing evidence of the formation of hydrogen bonds between the OH groups on the HA surface and the N—H groups of the PU polymer. Moreover, the chemical linkages between the OH groups on the surface of the HA nanocrystals and the N—C═O groups of PU were evident in the FTIR spectra of the composite membranes. The PU membranes typically became more hydrophilic after crosslinking with HA. The applicability of the prepared composite membrane was tested with salt aqueous solutions to test its suitability for wastewater treatment. With increased HA loading, the water flux increased from 392.1 to 1110.7 L $m^{-2} \cdot h^{-1}$, and all R rates exceed 81% and reached a value of 97.1% for the PHM-50 sample. The results show that the nanohydroxyapatite–PU MMMs have great potential application in water desalination.

REFERENCES

1. Koltuniewicz, A.; Drioli, E. In Membranes in Clean Technologies: Theory and Practice; Wiley-VCH: Weinheim, **2008**; Vol. 1, Chapter 1, p 1.
2. Khulbe, K. C.; Feng, C. Y.; Matsuura, T. In Synthetic Polymeric Membranes: Characterization by Atomic Force Microscopy; Springer: Berlin, **2008**; p 5.
3. Altinkaya, S. A.; Bulent, O. *J. Membr. Sci.* **2004**, *230*, 71.
4. Yamamura, H.; Kimura, K.; Watanabe, Y. *Environ. Sci. Technol.* **2007**, *41*, 6789.
5. Ng, L. Y.; Mohammad, A. W.; Leo, C. P.; Hilal, N. *Desalination* **2013**, *308*, 15.
6. Vinh-Thang, H.; Kaliaguine, S. *Chem. Rev.* **2013**, *113*, 4980.
7. Dong, G.; Li, H.; Chen, V. *J. Mater. Chem. A* **2013**, *1*, 4610.
8. Chung, T. S.; Jiang, L. Y.; Li, Y.; Kulprathipanja, S. *Prog. Polym. Sci.* **2007**, *32*, 483.
9. Vu, D. Q.; Koros, W. J.; Miller, S. J. *J. Membr. Sci.* **2003**, *211*, 311.
10. Jia, M.; Peinemann, K. V.; Behling, R. D. *J. Membr. Sci.* **1991**, *57*, 289.
11. Aroon, M. A.; Ismail, A. F.; Matsuura, T.; Montazer-Rahmati, M. M. *Sep. Purif. Technol.* **2010**, *75*, 229.
12. Hoek, E. M. V.; Ghosh, A. K.; Huang, X.; Liong, M.; Zink, J. I. *Desalination* **2011**, *283*, 89.
13. Wang, Z. F.; Wang, B.; Ding, X. M.; Zhang, M.; Liu, L. M.; Qi, N.; Hu, J. L. *J. Membr. Sci.* **2004**, *241*, 355.
14. Hassanajili, S.; Khademi, M.; Keshavarz, P. *J. Membr. Sci.* **2014**, *453*, 369.
15. Kamişoğlu, K.; Aksoy, E. A.; Akata, B.; Hasirci, N.; Baç, N. *J. Appl. Polym. Sci.* **2008**, *110*, 2854.
16. Ciobanu, G.; Carja, G.; Ciobanu, O. *Micropor. Mesopor. Mater.* **2008**, *115*, 61.
17. Ciobanu, G.; Carja, G.; Ciobanu, O. *Mater. Sci. Eng. C* **2007**, *27*, 1138.
18. Elliott, J. C. Structure and Chemistry of the Apatites and Other Calcium Orthophosphates; Elsevier: Amsterdam, **1994**.
19. Bazargan-Lari, R.; Bahrololoom, M. E.; Nemati, A.; Salehi, Z. *J. Food Agric. Environ.* **2011**, *9*, 652.
20. Ciobanu, G.; Ilisei, S.; Harja, M.; Luca, C. *Sci. Adv. Mater.* **2013**, *5*, 1090.
21. Bowen, W. R.; Mukhtar, H. *J. Membr. Sci.* **1996**, *112*, 263.
22. Raynaud, S.; Champion, E.; Bernache-Assollant, D.; Laval, J. P. *J. Am. Ceram. Soc.* **2001**, *84*, 355.
23. Lopes, M. A.; Monteiro, F. J.; Santos, J. D.; Serro, A. P.; Saramago, B. *J. Biomed. Mater. Res.* **1999**, *45*, 370.
24. Bengtsson, Å.; Sjöberg, S. *Pure Appl. Chem.* **2009**, *81*, 1569.
25. Kesting, R. E. Synthetic Polymeric Membranes—A Structural Perspective; Wiley-Interscience: New York, **1985**.
26. Ishikawa, T.; Wakamura, M.; Kondo, S. *Langmuir* **1989**, *5*, 140.
27. Mahajan, R.; Burns, R.; Schaeffer, M.; Koros, W. J. *J. Appl. Polym. Sci.* **2002**, *86*, 881.
28. Jia, M.; Peinemann, K. V.; Behling, R. D. *J. Membr. Sci.* **1992**, *73*, 119.

29. Hassanajili, S.; Khademi, M.; Keshavarz, P. *J. Membr. Sci.* **2014**, *453*, 369.
30. Wang, N.; Burugapalli, K.; Song, W.; Halls, J.; Moussy, F.; Zheng, Y.; Mac, Y.; Wu, Z.; Li, K. *J. Membr. Sci.* **2013**, *427*, 207.
31. Yu, L. Y.; Xu, Z. L.; Shen, H. M.; Hu, Y. *J. Membr. Sci.* **2009**, *337*, 257.
32. Chen, S.; Li, L.; Zhao, C.; Zheng, J. *Polymer* **2010**, *51*, 5283.
33. Mu, T.; Cong, Y.; Wang, W.; Zhang, B. *Desalination* **2012**, *298*, 67.
34. Peng, X.; Jin, J.; Yoshimichi, N.; Takahisa, O.; Izumi, I. *Nat. Nanotechnol.* **2009**, *4*, 353.
35. Dalwani, M.; Benes, N. E.; Bargeman, G.; Stamatialis, D.; Wessling, M. *J. Membr. Sci.* **2011**, *372*, 228.
36. Jiang, J. H.; Zhu, L. P.; Li, X. L.; Xu, Y. Y.; Zhu, B. K. *J. Membr. Sci.* **2010**, *364*, 194.